Development of a Docking Solution for Autonomous Vehicles

Miguel Duarte Castanheira Rodrigues Dias
miguel.rodrigues.dias@tecnico.ulisboa.pt

Instituto Superior Técnico, Universidade de Lisboa, Lisboa, Portugal

January 2021

Abstract

Docking systems represent a response to a growing need of connecting autonomous vehicles to each other or to fixed points to create networks of shared information or simply charge the devices. The lack of a mechanical system that fulfils these tasks, suitable for implementation in several vehicles was the starting point and the studied premise of this thesis. To develop the solution, a creative process was applied to devise alternative concepts, from which the most innovative and with more potential for performance was chosen. The concept was then subjected to structural testing in its critical components by static load simulations with the finite element method. The possibility of a transversal product to different vehicle classes was evaluated, with the help of a developed computational tool. Three different use cases were tested, corresponding to small satellites, autonomous underwater vehicles and vertical take-off and landing vehicles. Finally, one of the three finalized designs was chosen and implemented in a drone's dynamical model and the guidance of the vehicle was simulated, using optimal control techniques, to represent a docking operation. The finalized mechanism is innovative and modular and has potential for further development. Its main characteristics are its androgynous interface, peripheral capture capacity, large tolerance to misalignment and relative autonomy from the guidance of the vehicle. Testing showed that the final design was able to support loads correspondent to the projected worst-cases scenarios for the three applications. In the guidance simulation, the chosen vehicle was controlled accurately remaining inside the established margins.
Keywords: Docking Systems, Androgynous Interface, Peripheral Capture, Mechanical Design

1. Introduction

Docking systems enable the connection of vehicles to each other or to fixed points to create networks of shared information or to simply charge the devices and have seen their greatest development in the space industry [1]. Primarily serving as a port for the mechanical connection of two bodies, they can also enable transfers of energy, fluids or in the case of large spacecraft, crew.

In recent years, the predominant usage of docking mechanisms in space has shifted from larger to smaller spacecraft, for example the CubeSat standard satellite family [2]. This is due to increasing research projects involving the creation of networks of autonomous satellites [3] and also due to the still prohibiting cost of placing an object into orbit, which promotes phased launches and consequentially creates the need to assemble the objects into larger structures, leading to the creation of several docking mechanisms for small footprint satellites [4, 5, 6]. These mechanisms have seen developments in marine technology as well, especially in AUVs [7, 8, 9], whose autonomy is dependent on their ability to establish a connection with underwater docking stations or with each other to charge or exchange information. In Urban Air Mobility (UAM), a rising industry [10], docking systems will also be essential in the next years, since UAM is set to be based on the premise of autonomous VTOLs performing unmanned passenger transfers between fixed points in cities, and therefore the connection of these vehicles with the stations will be ensured by a type of docking mechanism.

These industries' versions of docking mechanisms do not have similar designs, since they were all created with their specific constraints in mind. Figure 1 and 2 show, respectively, a docking station of an AUV and of a small satellite. Along with their environment-dependent designs, most employ a gendered configuration, which prohibits the connection between equal interfaces and therefore forbids a connection between the same class of vehicles. Also, the majority do not have a peripheral capture mechanism, which enables an easy implementation of a port for energy/fluid transfer or additional modules for specific applications.

The purpose of this work is to develop a mechanism with these features and with a modular design,

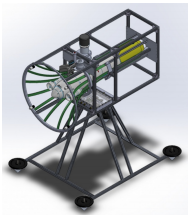

Figure 1: 3-D drawing of an AUV docking station [11].

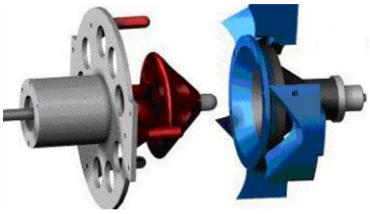

Figure 2: Design of a docking mechanism for small satellites [12].

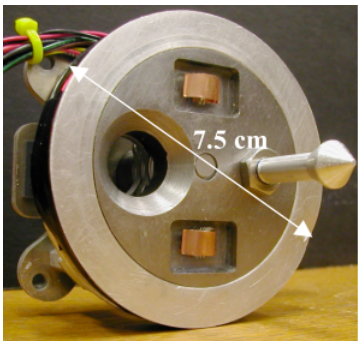

Figure 3: UDP mechanism.

enabling it to scale for different needs, more specifically, different load cases that represent the three aforementioned applications: small satellites, AUV and VTOL.

This paper details the development and the creative process implemented to devise preliminary designs and reach a finalized concept. The geometry and assembly properties of the designed mechanism were studied to define through general values the dimensions that describe the mechanism, correspondent to critical values of the structure, such as its outer diameter. The design was then tested in simulation with static stability analyses made on its critical components. The simulations were then replicated for the scaled components to simulate worst load case scenarios in the functioning of the mechanism for its intended applications. Finally, to implement one of the use cases in a simulated docking operation, a drone was selected, and with its model, altered to include the developed docking mechanism's characteristics, was created an optimal control strategy for the following of a designed trajectory, representative of a docking manoeuvre.

2. Background

In this section two relevant docking mechanisms within the context of this work are analysed and the principles for the structural analysis performed in the work are briefly summarized.

2.1. Relevant Docking Mechanisms

Because of the recent surge in research projects for docking mechanisms in small satellites, these were the primary focus in the literary research for this work. The state-of-the-art mechanism in this industry is the Universal Docking Port (UDP), shown in figure 3, developed by the Massachusetts Institute of Technology (MIT). This device has been tested aboard the International Space Station with success [13].

Its positive feature are its androgyny (the ability to connect with an equal interface), small footprint, low production cost, easiness of operation and no exposed moving parts. Nevertheless, it depends greatly on the previous alignment of the vehicles, because of its small size, and therefore small error margin, only permits one configuration to connect, and has limited space for connections, other than mechanical.

The Semi-Androgynous Mechanism (SAM) [5] developed in the Centro d'Ateneo di Studi e Attività Spaziali (CISAS) is also intended for small satellites. It explores the concept of semi-androgyny: one of the interfaces is able to change shape while the other receives it, maintaining its form. Figure 4 shows a schematic that illustrates the working principle of the mechanism.

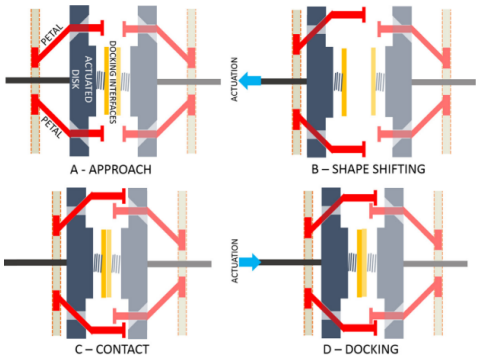

Figure 4: Simplified illustration of the connection process in the SAM.

Its main advantages are its androgyny, low footprint and cost and effective final alignment of the interfaces with the usage of electromagnets. However, this concept would not support large loads, due to its general polymeric composition. Since it was produced through additive manufacturing, its parts are complex and therefore harder to manufacture utilizing other processes.

The drawbacks of both mechanisms lowers their usability in different environments. Notwithstanding, both explore concepts to increase modularity for docking mechanisms for small satellites.

2.2. Structural Analysis

To structurally validate the mechanism, several linear static load analyses were performed. The method assumes: (1) loads are static (do not change in time) and are evenly distributed through the load area, (2) materials of the subjects are isotropic and (3) results are valid if the stress does not surpass the yield strength of the material.

The main metric chosen for the analysis was the von Mises stress $\bar{\sigma}_V$, defined by the following equation for multi-axial load, where σ_i represents the principal stresses:

$$\bar{\sigma}_V = \sqrt{\frac{1}{2}[(\sigma_1 - \sigma_2)^2 + (\sigma_2 - \sigma_3)^2 + (\sigma_3 - \sigma_1)^2]} \quad (1)$$

3. Methodology

This section details the process employed for the concept's design and validation.

3.1. Design

Since the product was created for the verification of the initial premise presented in this paper, no hard constraints were considered, such as price or size. Nevertheless, and since this research was done inside the thesis program of CEiiA (Centro de Excelência para Inovação da Indústria Automóvel), the design of the system follows generic constraints of the company, namely the qualifications of the production staff, available machinery and materials and guidelines provided by the engineering team.

To create the product to validate this paper's proposition, a creative process was implemented, inspired by two existing methodologies [14, 15]. The flow used in this work is summarized in figure 5.

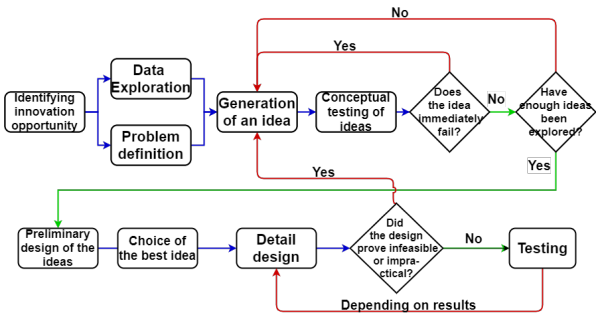

Figure 5: Utilized creative flow.

The following aspects were established as the desired features of the mechanism. The review of existing solutions and the requirements of the product, namely its ability for a cross platform implementation led to the choice of these characteristics.

- Low Footprint – To mitigate negative effects to the carrier of the mechanism derived from its adoption, such as unbalancing its centre of mass, inertia or drag coefficient;
- Simplicity – Namely low part count with low number of features and less active components (actuators and sensors);
- Modularity – Ability of a product or system within an initial design and assembly, to change components, adapt the usage of components of other designs, their dimensions or form to comply to different applications [16], essential for a transversal product;
- Misalignment Tolerance – The mechanism must still achieve connection, even if it is not perfectly aligned with the opposite interface, the value of the allowed misalignment should be as high as possible;
- Safety – Taking in consideration the possible hazardous effects of the environments of its applications, the system must not suffer permanent deformations or break in its operation;
- Symmetry – Depending on the number of axes of symmetry of the solution, it might have more than one connection configuration, increasing usability;
- Androgyny – An androgynous interface can connect with an equal interface which makes possible the connection between vehicles of the same category;
- Peripheral Capture - A peripheral capture/locking in the case of this product is desired to create a vacant central space in the mechanism for extra modules and ports.

Table 1 combines all of the aforementioned features and their conflicts with each other, "low" and "high" correspond, respectively, to low and high conflicts and "0" represents a pair that, in principle will not conflict or might benefit with the association.

The preliminary designs of the mechanisms included only the capture/mechanical guidance interfaces, since it is usually the main differentiator between different designs and is the first physical part of the system that is activated. The chosen mechanism was later upgraded to include the remaining subsystems. The designs were made in a computer aided design (CAD) program.

Three alternatives were devised with focus on different sets of the previously enumerated features. The first with focus on peripheral capture and androgyny, but lacking on the remaining features,

Table 1: The conflict matrix of the desired main features of the product. Abbreviations: "Foo"- footprint, "Sim" - simplicity, "Mod" - modularity, "Tol" - misalignment tolerance, "Saf" - safety, "And" - androgyny, "Sym" - symmetry, "Per" - peripheral capture

	Per.	Sym.	And.	Saf.	Tol.	Mod.	Sim.	Foo.
Foo.	High	0	0	High	High	Low	Low	
Sim.	High	Low	High	Low	Low	High		
Mod.	0	Low	0	High	0			
Tol.	Low	0	0	0				
Saf.	0	0	Low					
And.	0	High						
Sym.	0							
Per.								

namely safety. The second mechanism, on the other hand, excelled in its simplicity, having a low part count, with parts of general simple manufacture, it also had full rotational symmetry; however, it was not androgynous. The final solution encompassed features from both prior mechanisms, being androgynous with peripheral capture, with less safety issues as the first, nevertheless, more complex than the previous two.

Having finalized three preliminary designs, the more adequate in the context of this work was selected with the Analytic Hierarchy Process [17]. The chosen solution then suffered necessary alterations to finalize the concept, namely the addition of a locking sub-mechanism and various simplifications, considering CEiiA's conditions.

3.2. Structural Validation

In an effort to increase the modularity of the solution, various equations were conceived that define all the dimensions of the components of the mechanism with the input of a few general dimensions. The latter values correspond to supplementary parts' dimensions, such as shaft or screw hole diameters as well as general dimensions of the mechanism, such as its outer diameter. The equations were implemented on a program developed in Python programming language, that receives as inputs the general dimensions defined by a user and updates the designs of the mechanism's components. The creation of this tool was driven by the necessity of a rapid change of dimensions in various parts of the mechanism to adapt to the needs of its many applications.

To infer the concept's capacity for a cross platform implementation, its behaviour under load was studied. The worst load case scenarios were envisioned for the critical components of the mechanism. Since the validation performed in this work intends to be a pre validation to demonstrate the mechanism's general capabilities, only static forces were considered for all the applications, with the force's values directly related to the weight of the vehicles at sea level. Table 2 shows the three applications with respective test loads and the chosen maximum side dimension for each different scale of the mechanism. General values of mass were selected that represent the category of vehicles of the use cases, the maximum dimension was chosen in conformity to the average size of said vehicles.

Table 2: Test loads for structural validation and maximum side dimension of the mechanism for its three applications

Category	**Mass (test load)**	**Max dimension of mechanism**
CubeSat	$10kg$ $(100N)$	$220mm$
AUVs	$200kg$ $(2000N)$	$350mm$
VTOLs	$1000kg$ $(10kN)$	$850mm$

Prior to the structural validation, materials were picked for the parts, the 7075-T6 alloy was chosen for all the tested parts, since it is a low density alloy, standard in aerospace applications with a high yield strength (in the metal sheets used having a minimum yield strength of 460 MPa [18]).

The analyses followed a three-phase methodology: (1) determining the load cases for each component, (2) simplifying the parts to avoid issues related to stress singularities and (3) conducting a mesh independence study for increased reliability of results. Some alterations were made to the parts in conformity to the obtained results.

To define the load cases, the functioning of the concept was analysed, identifying the moments of extra load application and the critical components involved in the docking procedure. Then, the boundary conditions of the static stability analyses were defined, namely the load areas and fixed points, the latter corresponding to the connection points of the component to the rest of the mechanism.

Testing was conducted initially for the small satellite use-case mechanism and was repeated for the components of the remaining mechanisms, obtained through the sizing tool mentioned before. The final dimensions for the remaining use-cases were obtained iteratively, with the principal criteria for acceptance being the maximum von Mises stress in the component staying below the yield strength of the selected material.

3.3. Control Validation

To further validate the concept, a drone was considered as the carrier of the mechanism and docking vehicle and a trajectory was devised to represent a docking manoeuvre. The chosen drone was the

AR2.0 model from Parrot, whose main characteristics can be found in table 3, the availability of a dynamical model already implemented and evaluated [19] led to the choice of this device.

Table 3: AR2.0 Drone parameters.

Parameter	Notation	Value
Mass	m	475 g
xx Moment of Inertia	I_{xx}	2.2×10^{-3} $kg.m^2$
yy Moment of Inertia	I_{yy}	2.5×10^{-3} $kg.m^2$
zz Moment of Inertia	I_{zz}	4.5×10^{-3} $kg.m^2$
Arm Length	L	0.177 m
Thruster Force Constant	K_T	9.2×10^{-6} $N(rad/s)^{-2}$
Momentum Constant	K_T	0.32×10^{-6} $Nm(rad/s)^{-2}$
Voltage Constant	K_ω	0.002 $(rad/s)^{-1}$

The mechanism of the small satellite use-case was utilized in this experiment. For this segment of the work, the material considered for most of the mechanism shifted to the acrylonitrile butadiene styrene (ABS) polymer, a common additive manufacturing (AM) material with a relatively high yield strength to other polymers used in AM . This was done to test a version of the concept that would be readily available for an experiment in a real environment, since manufacturing the components through this process would be easier than machining them for a first prototype. Considering this material also permitted the creation of a base that would be harder to manufacture in any other process if not by AM.

This base was created to accommodate the necessary active parts of the mechanism and was designed to align its center of mass to its geometric center, for easier implementation. The mass, center of mass and inertia tensor of the mechanism with the added base and active components were obtained through the modelling software. These values were implemented in the dynamical model of the drone, now including the mass and inertia tensor of the drone+mechanism aggregate body.

A trajectory was defined that intends to simulate a standard docking procedure, composed of three manoeuvres:

1. Rise of the vehicle, representing the start of the movement;

2. Forward and side movement, to simulate the search and finding of the docking system;

3. Lowering of the drone, at a slowed pace to ensure an optimal capture.

To optimally control the following of the trajectory the Linear Quadratic Regulator technique and the Kalman filter algorithm were applied. A Kalman Filter was used since sensor noise was included in the simulated environment, the variance of the added noise can be seen in table 4, where P_x, P_y and P_z represent the drone's x, y and z position coordinates in the inertial frame ϕ, θ and ψ represent respectively, the roll, pitch and yaw angles (the attitude of the drone) in respect to the inertial frame. The tunable parameters of the controller were chosen iteratively to obtain the best possible following and ignoring for the most part the cost associated with the activation of the drone's motors.

Table 4: Variance of the added sensor noise

Output	**Variance**
P_x	7.3221×10^{-4}
P_y	4.2829×10^{-4}
P_z	1.8000×10^{-4}
ϕ	3.4817×10^{-4}
θ	2.6060×10^{-4}
ψ	3.8313×10^{-5}

4. Results

This section shows the achieved final design of the concept and the explanation of its working principle, the results of the structural analyses made on its critical components and the three finalized mechanisms' general characteristics. Lastly, the outcomes of the trajectory following are presented.

4.1. Final Design

Figure 6 shows the finalized design of the mechanism. It is fully androgynous, meaning that the two interfaces of the docking procedure would have the same design. It is composed of four "petals" which are fixed on a base, referred as the inner disk and are able to rotate through the vertical movement of an outer disk, which moves a shaft inside a slotted hole of the petals. The concept also employs four pairs of mirrored "guiding plates", around the periphery of the design. Between these plates are four "blockers" with springs attached. Below the outer disk are connected four radially equidistant components, referenced as the "unblockers", whose sole application is to open the blockers. Finally, in the top centre of the design is a locking disk.

Docking with this concept would be achieved in the following order of events:

1. The petals would rise with the lifting of the outer disk (limited to vertical movement) by one or a set of actuators;

2. The interfaces would align with the petals' interaction with the guiding surface, whose slope would make the petal slide until reaching the gaps designed to house them;

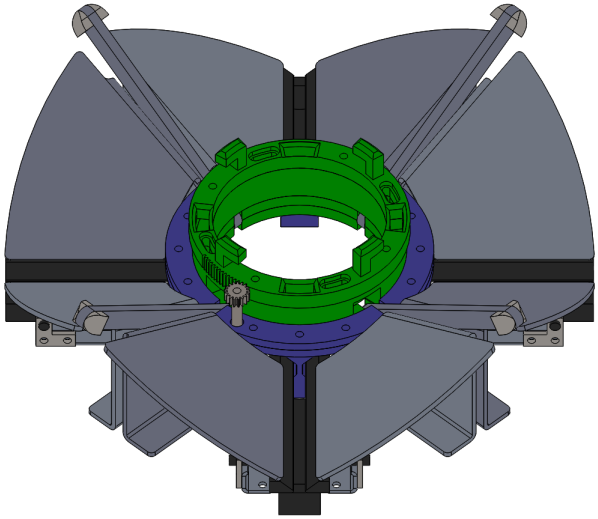

Figure 6: Final mechanism's CAD design (small satellite iteration).

3. With the tip of the petal inside the gap, its shape would open the blockers compressing the springs attached to them. After the top of the petal has entered completely, the blockers would close with the decompression of the springs. Capture would occur with the blocking of all the petals;

4. The outer disk lowers, lowering the petals, each sliding in the gaps, and closing the distance between the two interfaces;

5. Since there is a surface in the outer edge of the gap, the petal movement would stop when it would reach said surface aligning the interfaces;

6. This alignment would result on the locking disk connecting with the same part of the opposite mechanism, the disk of either interface would rotate with a motor to lock the mechanisms.

Undocking would occur with the rotation of the locking disk in the opposite direction, the rise of the outer disk (rising the petals) to separate the interfaces, then the rise of the outer disk of the opposite interface, which would open that interface's blockers and release the petals, separating the interfaces.

As desired, this concept employs a large central space free for modules such as ports for electrical connections or fluid transfers, sensors or extra locking components. This mechanism's movements would be controlled by two active components, an actuator, responsible for the movement of the outer disk and a motor, responsible for the rotation of the locking disk. After the petals of an interface are captured by the opposite interface, the rest of the docking operation would be conducted solely by the mechanism, saving resources of the vehicles that would be otherwise used in the close-range guidance phase of the docking procedure. The concept's misalignment tolerance would theoretically be large (a definite value would require experimental tests).

4.2. Linear Analyses Results

As mentioned, the criteria for the acceptance of the results was the maximum von Mises stress staying below the yield strength of the considered material, guaranteeing that no segment of the studied part suffers plastic deformation in its worst-case scenario. Since the stress distribution is similar in the same component in the different mechanisms, only one plot of a different mechanism for the three components will be presented.

Guiding Plate (GP) - In the first moments of docking, the petal might impact the guiding plate with the weight of the mechanism, the worst-case scenario envisioned in the usage of this part corresponds to the entirety of the weight of the vehicle submitted downwards in the middle of the outer edge of the plate. Figure 7 shows the stress plot of this part for the small satellite use case.

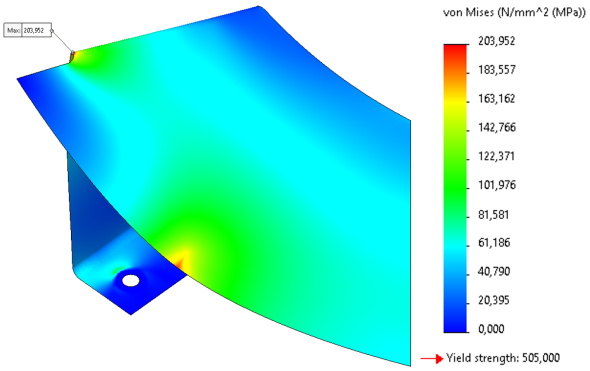

Figure 7: Stress plot of the GP in the small satellite mechanism (deformation scale of 5).

Petal - Between the capture of the petals and the locking of the mechanisms, these components might need to support the weight of the vehicle, depending on the location of the mechanism in the chaser and target bodies. This case considers an equal distribution of the load between the four petals, so a quarter of the load is applied transversely to the part. Figure 8 shows the stress plot of the petal for the mechanism designed for the AUV, with the right arrows showing the location of the application of load.

Locking Disk (LD) - This part is activated in the locking of the mechanism, being the most crucial component to analyse, seeing that it will endure the connection load for a prolonged period. Figure 9 shows the component's stress plot for the VTOL mechanism, where the load is applied perpendicularly to the axis of revolution of the disk.

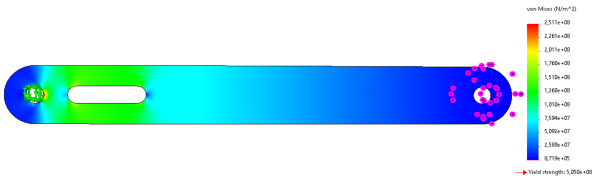

Figure 8: Stress plot of the Petal in the AUV mechanism (deformation scale of 7).

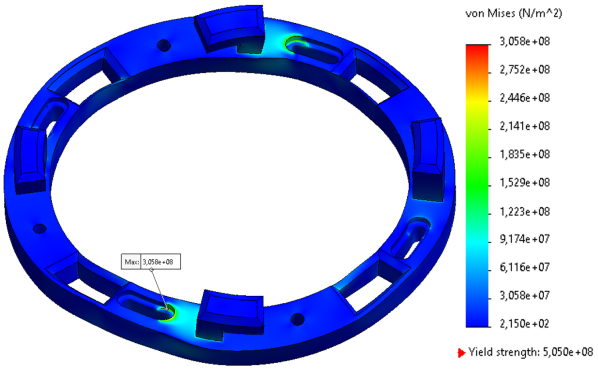

Figure 9: Stress plot of the LD in the VTOL mechanism (deformation scale of 100).

Table 5 summarizes the results of the stress tests of the three components and shows the final mass, maximum dimension, central diameter and misalignment tolerance for each mechanism. The mass was calculated through the modelling software. The misalignment tolerance is theoretical, since this feature would need to be tested experimentally for an accurate measurement. This value was obtained by analysing the dimensions, namely the span of the petals and the maximum diameter of the mechanism and represents the maximum distance between the two participant mechanisms' geometric centres, where docking would theoretically still occur. Figure 10 shows a schematic for visual support on how this value was calculated.

Table 5: Stress tests results and characteristics of the final designs of the three use case mechanisms considering the 7075-T6 alloy ($\sigma_y > 460$ MPa) for the three tested components

		SmallSat (10 kg)	**AUV (200 kg)**	**VTOL (1000 kg)**
Max. Stress	GP	204.0 MPa	375.3 MPa	430.4 MPa
	Petal	316.47 MPa	268.8 MPa	374.1 MPa
	LD	39.91 MPa	207.0 MPa	305.8 MPa
Mass		732.43 g	5231.19 g	38624.21 g
Mass Ratio		7.32 %	2.62 %	3.86 %
Maximum Side		220 mm	350 mm	850 mm
Central Diameter		65 mm	108 mm	220 mm
Axial Misalignment Tolerance		29.8 mm	45.00 mm	122.9 mm

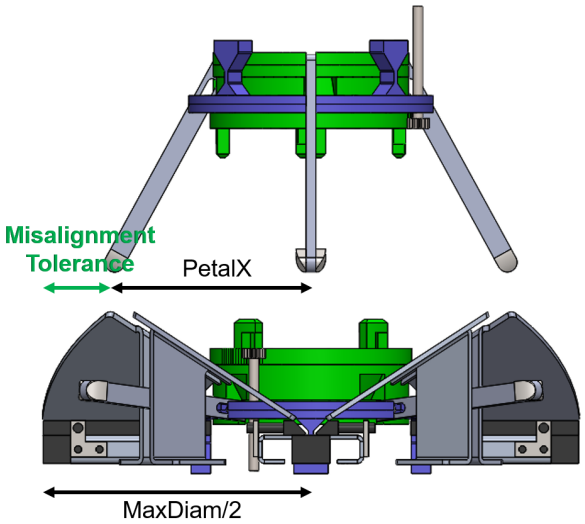

Figure 10: Visual aid to calculate the misalignment tolerance: A mechanism (without its outer components) approaching another mechanism to connect.

The stress tests showed that the mechanism was able to support, in its critical parts, the projected loads, as the maximum stress for every test stayed below the yield strength of the material. The value of the yield strength of the used alloy is not independent of the dimensions of the mechanism, but its minimum value was considered to be 460 MPa [18]. Since the small satellite mechanism was the first to be designed, suffered more alterations to optimize its results, the remaining were iteratively redesigned to achieve maximum stress below the considered yield strength. The fidelity of the results was confirmed by mesh independence studies.

4.3. Trajectory Following Results

The final mechanism considered for this application is shown attached to the 3-D model of the AR2.0 drone in figure 11. It was allocated in the bottom of the drone since the vehicle favours vertical movements, therefore, docking would be optimal if performed with the lowering of the airborne drone. The mechanism was positioned so its centre of mass (CM) would be in the same axis as the drone's CM.

The overall mass, $0.696kg$, was obtained adding the mass of the drone to the mass of the mechanism with the added parts (base, actuator and motor), $0.221kg$, which was obtained from the modelling software. The inertia tensor of the mechanism was obtained through the modeller as well and applying the parallel axis theorem to the inertia tensor of the drone, the inertia of the aggregate body was obtained:

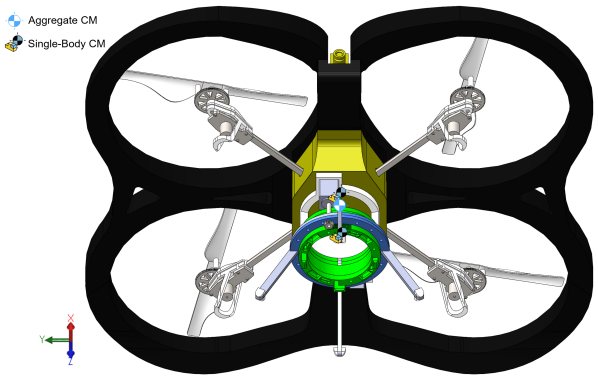

Figure 11: Mechanism attached to the drone, showing individual and aggregate CM.

$$I_{set} = \begin{bmatrix} 2.73 & 0 & 0 \\ 0 & 3.54 & 0 \\ 0 & 0 & 5.01 \end{bmatrix} \times 10^{-3} \quad kgm^2 \qquad (2)$$

Figure 12 shows the following of the simulated trajectory of drone+mechanism system compared to the reference trajectory.

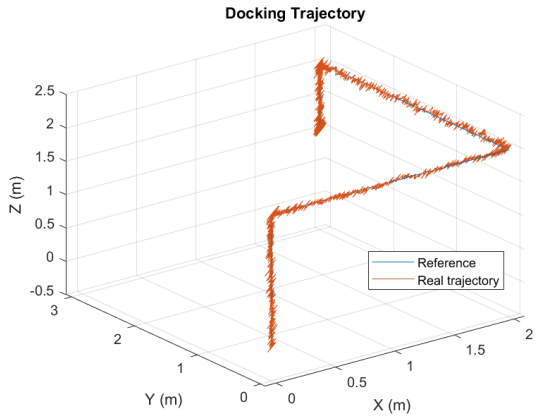

Figure 12: Reference and simulated trajectory in a 3-D plane.

To validate the simulated guidance of the drone the mean absolute error (MAE) was used:

$$MAE = \frac{\sum_{i=1}^{n} |\hat{P}_i - P_i|}{n} \qquad (3)$$

where $\hat{P}_i$ and P_i represent the position coordinates of the simulation and of the trajectory, respectively, and n is the number of measured time samples. These values were calculated for the final manoeuvre of the trajectory.

The XY plane of this experiment corresponds to the ground plane, therefore, the P_x and P_y MEA values should be analysed. The module of the vector formed by these distances would correspond to the distance between the axes of revolution of the two connecting interfaces, equal to the maximum misalignment. The obtained value was 24.8 mm, inside the established tolerance of 29.8 mm.

To simulate real conditions, sensor noise was added, as previously mentioned, which led the obtained deviations to be close to the error margin, yet, the average misalignment did not surpass it. In addition, since the concept was designed to align itself in the presence of misalignment, this approach is a valid first control strategy suitable for implementation in a controlled environment with the considered drone and mechanism.

5. Conclusions

The development of the present research culminated in a concept with an androgynous design, a peripheral capture interface, able to connect in four different configurations (rotating the mechanism $90n$ degrees) and was designed with a modular basis for adaptability between use cases. The concept also possesses a large misalignment tolerance, which is for now theoretical and should be confirmed in future experiment tests. Its size and mass are its biggest disadvantages, however the interface was designed to have the possibility to be either passive or active, so removing certain parts would not compromise its performance and would reduce further its footprint.

The stress results show the applicability of the design for the three cases. This should be treated as a pre validation, and should be continued for future applications of the developed concept. Nevertheless, the hypothesis of a modular design for a transversal docking mechanism was verified.

A trajectory was defined and validated with the application of optimal controllers and observers designed for the best possible following of the trajectory. The cost of the usage of the drone's motors was neglected, in other situations such as docking in space, a more conservative approach to the actuation of the thruster might be warranted, to limit fuel consumption. The results of this segment showed that the position error was under the established misalignment tolerance, therefore, in real conditions the docking is expected to occur normally. This trajectory following intends to represent a controlled docking without process noise, so it would be optimal for a future testbed of the mechanism in a closed environment.

Acknowledgements

This work was supported by CEiiA's MSc thesis program.

References

[1] John Cook, Valery Aksamentov, Thomas Hoffman, and Wes Bruner. ISS interface mechanisms and their heritage. In *AIAA SPACE Conference and Exposition 2011*. AIAA, 2011.

[2] Armen Toorian, Ken Diaz, and Simon Lee. The CubeSat approach to space access. In *IEEE Aerospace Conference Proceedings*, 2008.

[3] Sharmila Padmanabhan, Shannon Brown, Pekka Kangaslahti, Damon Russell, Richard Cofield, Robert Stachnik, and Boon Lim. A 6U CubeSat constellation concept for atmospheric temperature and humidity sounding. In *2014 United States National Committee of URSI National Radio Science Meeting, USNC-URSI NRSM 2014*, aug 2014.

[4] Lennon Rodgers, Nicholas Hoff, Elizabeth Jordan, Michael Heiman, and David Miller. A Universal Interface for Modular Spacecraft. *Small Satellite Conference*, aug 2005.

[5] Lorenzo Olivieri and Alessandro Francesconi. Design and test of a semiandrogynous docking mechanism for small satellites. *Acta Astronautica*, 122:219–230, may 2016.

[6] Rebecca C Foust, Elena Sorina Lupu, Yashwanth Kumar Nakka, Soon Jo Chung, and Fred Y Hadaegh. Ultra-soft electromagnetic docking with applications to in-orbit assembly. In *Proceedings of the International Astronautical Congress, IAC*, volume 2018-Octob, pages 1–5, 2018.

[7] Brett W. Hobson, Robert S. McEwen, Jon Erickson, Thomas Hoover, Lance McBride, Farley Shane, and James G. Bellingham. The development and ocean testing of an AUV docking station for a 21" AUV. In *Oceans Conference Record (IEEE)*, 2007.

[8] Jonathan Evans, Paul Redmond, Costas Plakas, Kelvin Hamilton, and David Lane. Autonomous docking for intervention-AUVs using sonar and video-based real-time 3D pose estimation. In *Oceans 2003: Celebrating the Past... Teaming Toward the Future*, 2003.

[9] Szymon Krupiński, Francesco Maurelli, Angelos Mallios, Panagiotis Sotiropoulos, and Tomeu Palmer. Towards AUV docking on subsea structures. In *OCEANS '09 IEEE Bremen: Balancing Technology with Future Needs*, 2009.

[10] Christelle Al Haddad, Emmanouil Chaniotakis, Anna Straubinger, Kay Plötner, and Constantinos Antoniou. Factors affecting the adoption and use of urban air mobility. *Transportation Research Part A: Policy and Practice*, 132:696–712, feb 2020.

[11] Natàlia Hurtós, Angeles Mallios, Narcís Palomeras, Josep Bosch, Guillem Vallicrosa, Eduard Vidal, David Ribas, Nuno Gracias, Marc Carreras, and Pere Ridao. LOON-DOCK: AUV homing and docking for high-bandwidth data transmission. In *OCEANS 2017 - Aberdeen*, 2017.

[12] Jane C. Pavlich, Peter Tchoryk, Jr., Anthony B. Hays, and Gregory Wassick. KC-135 zero-G testing of a microsatellite docking mechanism. In *Space Systems Technology and Operations*, volume 5088, pages 31–42, 2003.

[13] Duncan Lee. *Development of Resource-Constrained Sensors and Actuators for In-Space Satellite Docking and Servicing m ,Signature redacted Signature redacted Signature redacted ,Signature redacted*. PhD thesis, 2015.

[14] Mike Baxter. *Product design*. CRC Press, 1995.

[15] J. Daniel Couger, Lexis F. Higgins, and Scott C. McIntyre. (Un)structured creativity in information systems organizations. *MIS Quarterly: Management Information Systems*, 17(4):375–394, dec 1993.

[16] Karl Ulrich. *Fundamentals of Product Modularity*, pages 219–231. Springer Netherlands, Dordrecht, 1994.

[17] TL. Saaty. Fundamentals of Decision Making and Priority Theory with the AHP. , Pittsburgh, PA, U.S.A. *RWS Publications*, VI, 1994.

[18] B S EN and Others. Aluminium and Aluminium Alloys- Sheet, Strip and Plate- Part 2: Mechanical Properties. 2013.

[19] Miguel Santiago, Guilherme Antunes, André Miranda, and David Ribeiro. UAV Red Bull Air Race 3rd Delivery Report - Group 13. Technical report, Instituto Superior Técnico, 2020.